Supramolecular Chemistry
Publication details, including instructions for authors and subscription information:
http://www.informaworld.com/smpp/title~content=t713649759

Spectroscopic studies on the cyclodextrin inclusion complexes of aromatic compounds and radicals

Makoto Aoyagi[ab]; Masafumi Ata[ac]; Yasuhiko Gondo[a]; Yoshihiro Kubozono[ad]; Yasunobu Suzuki[ae]
[a] Contribution from the Department of Chemistry, Faculty of Science, Kyushu University 33, Hakozaki, Higashiku, Fukuoka, Japan [b] Dainippon Printing Co., Ltd., Shinjukuku, Tokyo, Japan [c] SONY Central Research Center, Yokohama, Japan [d] Department of Chemistry, Okayama University, Tsushima, Okayama, Japan [e] Tokyo Gas Co. Ltd., Arakawaku, Tokyo, Japan

To cite this Article Aoyagi, Makoto , Ata, Masafumi , Gondo, Yasuhiko , Kubozono, Yoshihiro and Suzuki, Yasunobu(1993) 'Spectroscopic studies on the cyclodextrin inclusion complexes of aromatic compounds and radicals', Supramolecular Chemistry, 2: 4, 277 — 282
To link to this Article: DOI: 10.1080/10610279308029818
URL: http://dx.doi.org/10.1080/10610279308029818

SUPRAMOLECULAR CHEMISTRY, Vol. 2, pp. 277–282
Reprints available directly from the publisher
Photocopying permitted by *license only*

Spectroscopic studies on the cyclodextrin inclusion complexes of aromatic compounds and radicals

MAKOTO AOYAGI[†], MASAFUMI ATA[††], YASUHIKO GONDO*, YOSHIHIRO KUBOZONO[‡] and YASUNOBU SUZUKI[‡‡]

Contribution from the Department of Chemistry, Faculty of Science, Kyushu University 33, Hakozaki, Higashiku, Fukuoka 812, Japan

(Received July 30, 1992)

We have studied three different subjects, i.e., the ESR line-shape changes, induced circular dichroism (ICD), and suppression of fluorescence quenching, all caused by inclusion complex formation with cyclodextrins.

INTRODUCTION

We here report on our recent spectroscopic studies on the cyclodextrin inclusion complexes of aromatic compounds and radicals, focusing on the three different subjects, i.e., the ESR line-shape changes, induced circular dichroism (ICD), and suppression of fluorescence quenching, all caused by inclusion complex formation with cyclodextrins (CyDxs). We have found that the CyDx inclusion complex formation makes the ESR spectra of radical species very sharp and beautiful so that we can discuss such inclusion dynamics as the guest rotation in the CyDx cavity and the forward and reverse processes in the inclusion equilibrium, and we can also determine very small hyperfine coupling (hfc) constants. As for the ICD, we will point out the importance of this technique in the radical spectroscopy, where the physical significance is obviously the inducsion of the circular dichroism, while as important as the physical one is the chemical significance that the CyDx inclusion leads to generation of neat radicals. From the study on the inclusion suppression of the fluorescence quenching, we have found that surprisingly crucial is the solvent composition, which is seemingly interesting from the viewpoint of the solution chemistry.

[†]Dainippon Printing Co., Ltd., Shinjukuku, Tokyo 162-01, Japan. [††]SONY Central Research Center, Yokohama 240, Japan. [‡]Department of Chemistry, Okayama University, Tsushima, Okayama 700, Japan. [‡‡]Tokyo Gas Co. Ltd., Arakawaku, Tokyo 116, Japan.

RESULTS AND DISCUSSION

(1) ESR line-shape changes: inclusion dynamics and determination of very small hyperfine coupling constants

Figure 1(a) shows the ESR spectrum of the *p*-benzosemiquinone radical anion ($PBSQ^{-\cdot}$) in alkaline 95% ethanol, while Figure 1(b) shows that in alkaline aqueous solution containing α-CyDx; the former spectrum is normal in intensity distribution, whereas the latter is anomalous.[1] This anomaly comes from the inclusion complex formation, i.e., four protons are no longer equivalent, and are classified into two groups, which gives the last, cross term in eq 1. Owing to inclusion, the tumbling motion of the radical is somewhat suppressed so that the linewidths are expressed by

$$\Delta H(m_1^H, m_2^H) = A + B_1 m_1^H + C_1 (m_1^H)^2 + B_2 m_2^H + C_2 (m_2^H)^2 + D m_1^H m_2^H \quad (1)$$

where $\Delta H(m_1^H, m_2^H)$ is the peak-to-peak width of the line corresponding to the proton spin quantum number of group one, m_1^H, and that of group two, m_2^H. The coefficients A, B, and C are the constants determined by the anisotropic g tensors and anisotropic hyperfine splitting tensors of the two groups of protons as well as by the rotational correlation time. It may be noted that here is introduced a cross term with coefficient D. The individual lines represented by the proton spin quantum numbers m^H in the normal ESR spectrum are represented by the sets of (m_1^H, m_2^H), respectively; from the low-field to the high-field lines, they are $(-1, -1)$ for $m^H = -2$, $(-1, 0)$ and $(0, -1)$ for $m^H = -1$, $(0, 0)$, $(1, -1)$, and $(-1, 1)$ for $m^H = 0$, $(1, 0)$ and $(0, 1)$ for $m^H = 1$, and $(1, 1)$ for $m^H = 2$.

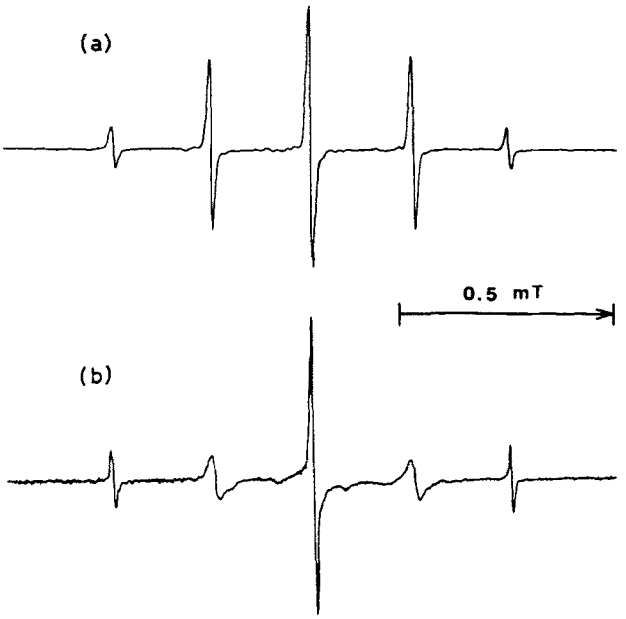

Figure 1 ESR spectra of $PBSQ^{-\cdot}$ in 95% ethanol (a) and in α-CyDx aqueous solution (b) observed at room temperature. The proton hfc constants are 0.231 (a) and 0.232 mT (b).

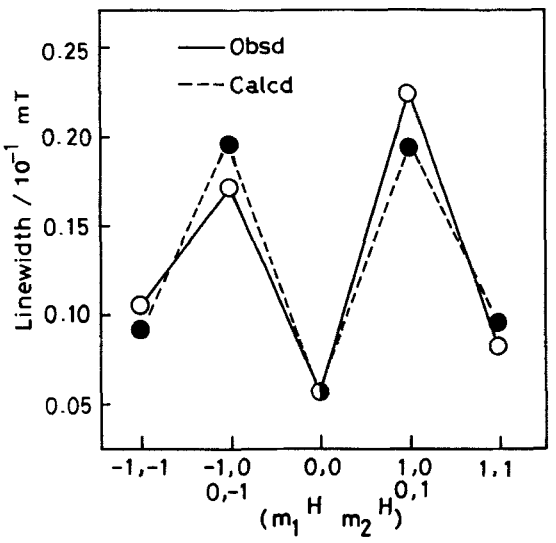

Figure 2 Comparison of the observed and calculated linewidths for the $PBSQ^{-\cdot}$ observed in α-CyDx aqueous solution. As for the sets of nuclear spin quantum numbers, see the paragraph associated with eq 1.

Figure 2 shows the linewidths observed and calculated with eq 1 by use of the least-squares method. In the absence of the anisotropic hyperfine splitting tensors, one cannot calculate linewidths from eq 1 directly, though the anisotropic g tensor is available.[2] Consequently, we have estimated the validity of eq 1 by comparing the lindwidths observed with those calculated by use of the coefficients determined by the least-squares method on the basis of the assumption that $B_1 = B_2$ and $C_1 = C_2$. In application of the least-squares method, we adopted the lines corresponding to the (m_1^H, m_2^H) sets of $(-1, -1)$, $(-1, 0)$, $(0, -1)$, $(0, 0)$, $(1, 0)$, $(0, 1)$, and $(1, 1)$.

Since the splitting in the sets of $(-1, 0)$ and $(0, -1)$ is not observed, we assume that for these sets the linewidths are practically equal and the line centers are very close to each other. Accordingly, the linewidths for these sets are regarded as equal to the observed apparent peak-to-peak width of the second left transition in Figure 1(b). A similar procedure is applied to the sets of $(1, 0)$ and $(0, 1)$, where the second right observed transition has offered the necessary linewidth. Furthermore, the linewidth of the central line for the set of $(0, 0)$ is taken as the peak-to-peak width of the most intense observed line. Thus, the five different linewidths derived straightforwardly from the apparent linewidths in Figure 1(b) are used for determination of the coefficients in eq 1. Around the most intense central line there must be two transitions corresponding to the sets $(-1, 1)$ and $(1, -1)$, which are estimated to have the linewidths about ten times as wide as that for the set $(0, 0)$ on the basis of eq 1, as detailed above; hence the central part of the observed spectrum can reasonably be interpreted to consist of a very sharp line and two broad lines.

As shown in Figure 2, excellent agreement has been obtained between the calculated and observed linewidths. This indicates that eq 1 is reasonable in the case of the $PBSQ^{-\cdot}$ – α-CyDx inclusion complex. Therefore, we conclude that the molecular rotation of $PBSQ^{-\cdot}$ is suppressed when it is included in α-CyDx cavity. In summary, the rotational tumbling of $PBSQ^{-\cdot}$ about the axis parallel to the symmetry axis of α-CyDx is rarely restricted, whereas that about the axis perpendicular to the symmetry axis is governed by the Brownian motion of the inclusion complex as a whole, similarly to the case of nitroxide radicals.[3] In order to interpret the ESR spectrum observed for $PBSQ^{-\cdot}$ included in α-CyDx, it seems interesting to study the effects of the two different groups of protons by use of partially deuterated PBSQ radical anions.

Figure 3 shows the ESR spectrum of nitrobenzene radical anion ($NB^{-\cdot}$) included in β-CyDx in 50% aqueous ethanol observed at 20°C, which manifests two characteristic features; first, the narrow and well-resolved lines especially in the central portion and secondly the asymmetry in linewidth and amplitude.[4] In general, the rapid passage of solvated ions by radicals and the collision among radicals affect the spin precession, resulting in the isotropic ESR line broadening. Thus, the narrow linewidths can be attributed to the suppressed collisions due to inclusion in the β-CyDx cavity. The unsymmetrical line feature is also an immediate consequence of the inclusion

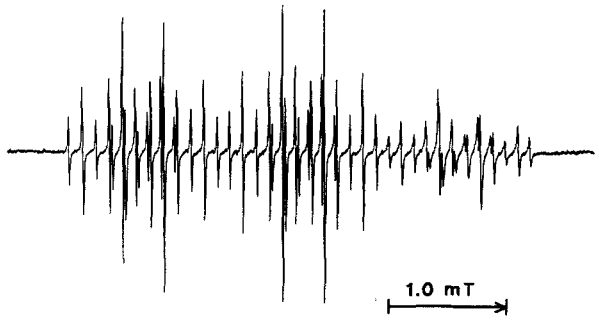

Figure 3 ESR spectrum of $NB^{-}\cdot$ included in β-CyDx in 50% aqueous ethanol observed at 20°C.

complex formation; the suppressed tumbling of the radical modulates the anisotropic g and hyperfine splitting A^N tensors, yielding the nuclear-spin-dependent linewidths. Since the tumbling modulation of the anisotropic g and A^N tensors modifies the transverse relaxation time and causes the nuclear-spin-dependent line broadening, the smallest effect of tumbling modulation is naturally found for the central-field lines associated with $m^N = 0$, where m^N stands for the ^{14}N nuclear spin quantum number. The rotational correlation time τ of the included $NB^{-}\cdot$ is estimated to be 5×10^{-11} s by use of eq 2,[5]

$$\tau = A_\tau \Delta H(+1)[(I(+1)/I(-1))^{1/2} - 1] \quad (2)$$

where A_τ is related to the anisotropies in the g and A^N tensors of $NB^{-}\cdot$,[6] $\Delta H(+1)$ is the peak-to-peak linewidth of the low-field line of $m^N = +1$, and $I(+1)$ and $I(-1)$ are the peak-to-peak heights of the lines of $m^N = +1$ and -1, respectively, all averaged over the para-proton doublets.[7]

Figure 4 shows the central portion of the ESR spectrum of nitrobenzene-d_5 radical anion (NB-$d_5^-\cdot$) and the simulated one with the ortho, meta, and para deuteron hfc constants of 53.8, 18.4, and 57.7 μT.[8] The deuteron hfc constants are practically consistent with the general proton-to-deuteron hfc ratio. Among the three envelopes associated with the $m^N = +1$, 0, and -1, the central one with $m^N = 0$ has the highest resolution; actually the hyperfine structures due to deuterons are not resolved in the high-field envelope of $m^N = -1$. Worthy of note, the β-CyDx inclusion complex formation makes it feasible to estimate the very small hfc constants of deuteron and remote protons in long alkyl substituents.[8]

Figure 5 shows the variations of the $N(+1)$ and $N(0)$ linewidths of methylviologen radical cation ($MV^{+}\cdot$) included in β-CyDx in 50% aqueous ethanol and those of $MV^{+}\cdot$ in absolute ethanol without β-CyDx.[9] Here $N(m^N)$ denotes an ESR line for which the nitrogen nuclear spin quantum number is m^N, while the resultant proton spin quantum number vanishes.

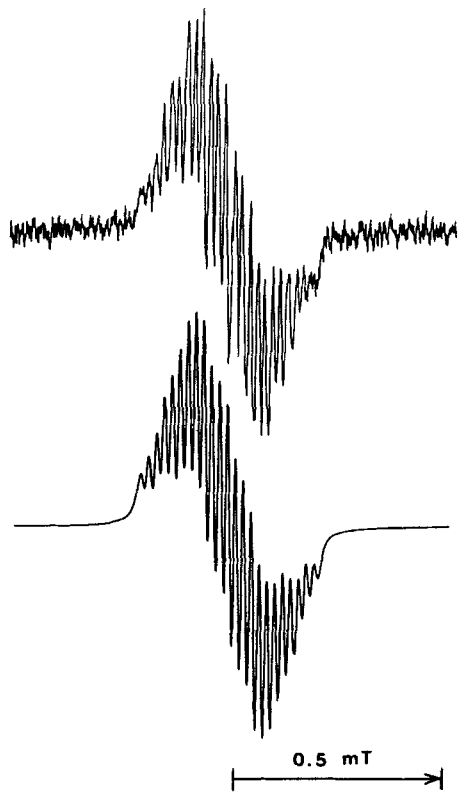

Figure 4 Central portion of the ESR spectrum of NB-$d_5^-\cdot$ included in β-CyDx in 50% aqueous ethanol observed at 20°C (upper) and that of the simulated one with Lorentzian line shapes (lower).

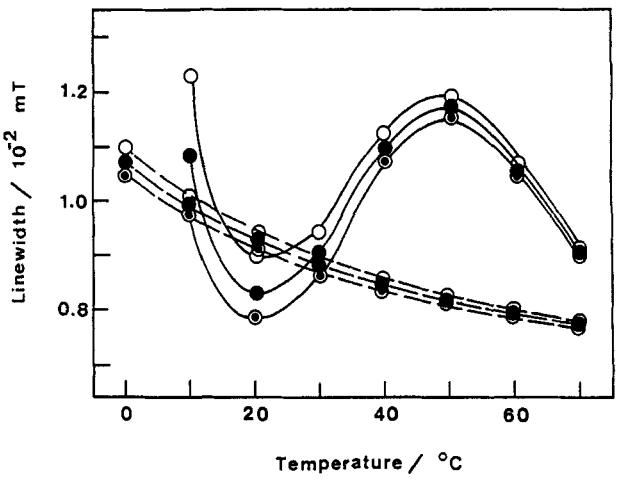

Figure 5 Temperature variations of linewidths in the ESR lines, N(+1) (●), N(0) (◉), and N(−1) (○) of $MV^{+}\cdot$ included in β-CyDx in 50% aqueous ethanol (full lines) and those of the inclusion-free radical cation in absolute ethanol (dashed lines). As for the notation $N(m^N)$, see text.

The motional narrowing is seen to develop monotonically with increasing temperature for the inclusion-free $MV^{+}\cdot$, whereas the temperature variation is sinuous for the included $MV^{+}\cdot$, suggesting that at least two competitive processes are involved. The decrease

in linewidth in the included $MV^{+\cdot}$ is seen from 10 to 20°C, which is ascribed to the increased motional narrowing with increasing temperature. The narrower linewidths for the included $MV^{+\cdot}$ than those for the inclusion-free $MV^{+\cdot}$, at about 20°C, are attributed to the inclusion-induced reduction of such perturbations as the spin-dipolar and spin-exchange interactions; the collisions with other radicals and solvated ions are effectively diminished when the radical is included. The increase in linewidth observed for the included $MV^{+\cdot}$ in the 20–50° region may be brought about by the increased rate of chemical exchange, i.e., the increased rates of the forward and reverse processes in inclusion equilibrium, which decreases the transverse relaxation time and gives rise to line broadening. This implies that the inclusion process is accompanied with thermal activation. The linewidth narrowing above 50°C is an indication of the motional narrowing predominating over the broadening due to the chemical exchange.

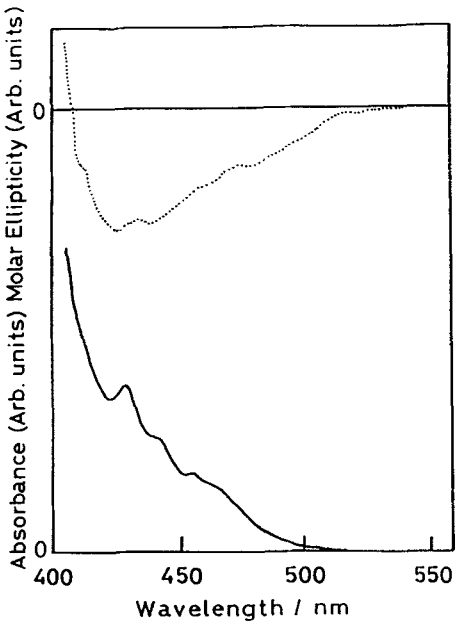

Figure 7 As in Figure 6, except that the radical is $NB^{-\cdot}$.

(2) Induced circular dichroism (ICD)

Figure 6 shows, as much as we know, the first observation of the ICD spectrum of a CyDx-included radical species, where the radical is the *N*,*N*′-dihydro-4,4′-dipyridinium radical cation ($DHDPY^{+\cdot}$) axially included in β-CyDx.[10] On the basis of the coupled oscillator model, the guest electronic transition polarized perpendicularly to the β-CyDx cavity axis exhibits negative ICD, whereas that polarized along the β-CyDx cavity axis exhibits positive ICD.[11,12] As shown in Figure 6, the ICD signs observed in the visible region are all positive, indicating that the two electronic absorption bands are polarized along the long molecular axis, in agreement with the molecular orbital calculations.[10]

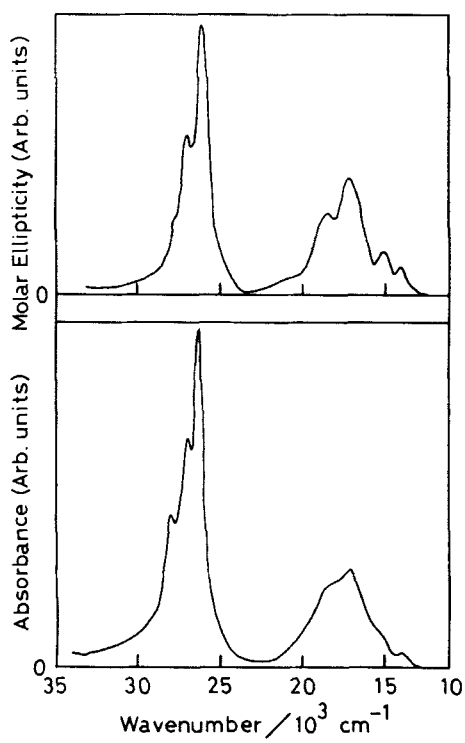

Figure 6 The ICD (upper) and electronic absorption (lower) spectra of the $DHDPY^{+\cdot}$ – β-CyDx inclusion complex in 50% aqueous ethanol observed at room temperature.

Figure 7 shows the ICD and absorption spectra of $NB^{-\cdot}$ included in β-CyDx in 50% aqueous ethanol observed at room temperature.[4] The observed negative ICD sign indicates that the absorption band tail covering the 410–500 nm region is polarized along the short molecular axis in accordance with the theoretical prediction.[13] The absorption spectrum of Figure 7 is different from that of the $NB^{-\cdot}$ generated by alkali metal reduction;[14] the former shows no absorption above 510 nm whereas the latter shows fairly broad band around 560 nm. Thus, the broad absorption bands in the visible region in the literature must be attributed to dianions or reaction products such as dimer and polymer produced by contact with alkali metal. The above mentioned two examples clearly show that the inclusion complex formation is significant for radical spectroscopy in the sense that the ICD is useful for assignment of electronic transitions and the inclusion complex formation serves to generate neat radicals.

(3) Suppression of fluorescence quenching by inclusion complex formation

We have studied the suppression of the pyrene (Py) fluorescence quenching by inclusion complex formation.[15] The host is β-CyDx, and the electron-transfer type quenchers studied are methylviologen (MV^{++}) and benzylviologen (BV^{++}) which are not included in β-CyDx. Table 1 shows the fluorescence decay constants k_0 of Py in the absence of the quenchers, first band-to-third band intensity ratios I_1/I_3, and the solvent viscosities η. From the I_1/I_3 ratios, as is well known, we see that the inclusion in 10% aqueous ethanol is well established. The Stokes' radii b are estimated to be 0.37, 0.36, 0.54, and 0,75 nm respectively for Py, MV^{++}, BV^{++}, and the inclusion complex Py–β-CyDx.[16]

Table II shows the fluorescence quenching rate constants k_q and the related parameters D' which are defined by

$$D' = \frac{1}{\eta}\left(\frac{1}{b(\text{fluorophore})} + \frac{1}{b(\text{quencher})}\right) \quad (3)$$

and are proportional to the sum of the diffusion coefficients of the fluorophore and quencher.[17] The fluorescence decay curves were observed with the peak heights of 10,000 counts, and are practically mono-exponential. In the absence of β-CyDx, the k_q values of MV^{++} and BV^{++} are comparable and proportional to the D' values, i.e., controlled by diffusion. On the other hand, in the presence of β-CyDx, the k_q values in 10% aqueous ethanol solutions are much smaller than those predicted by the D' values, showing efficient suppression of the fluorescence quenching by inclusion complex formation, in a contrast to the statement in the literature.[18] The effect of the bulky substituents in BV^{++} is also clearly seen through inclusion complex formation.

The significance of these observations are as follows; the electron-transfer type quenching is affected by the cyclodextrin inclusion, and hence the electron transfer efficiency is sensitive to the relative orientation of the fluorophore and quencher.

Table 1 Fluorescence decay constants k_0 and band intensity ratios I_1/I_3 of Py, and solvent viscosities η at 25°C

Solvent EtOH vol%	η / mPa s	[β-CyDx] / 10^{-2} M	I_1/I_3	k_0 / 10^6 s^{-1}
10	1.21	0	1.73	4.65
10	1.21	1.0	0.69	2.30
50	2.42	0	1.38	3.03
50	2.42	1.0	1.31	2.94

EXPERIMENTAL SECTION

Materials

p-Benzoquinone (Tokyo Kasei, EP) was sublimed under reduced pressure. α-CyDx (Tokyo Kasei, GR) was used as received. β-CyDx (Tokyo Kasei, GR) was recrystallized twice from distilled water and dried under vacuum at 80°C. Nitrobenzene (Tokyo Kasei, GR) was vacuum distilled. Nitrobenzene-d_5 (Aldrich, 99 atm% *D*) was used as received. 4,4′-Bipyridyl (Tokyo Kasei, GR) was recrystallized twice from ethanol (Wako, super special grade). 1,1′-Dimethyl-4,4′-dipyridinium (methylviologen; MV^{++}) dichloride (Tokyo Kasei, GR) and 1,1′-dibenzyl-4,4′-dipyridinium (benzylviologen; BV^{++}) dichloride (Tokyo Kasei) were recrystallized twice from ethanol (Tokyo Kasei, GR) and dried under vacuum. Pyrene (Wako, super special grade) was purified by column chromatography on silica gel (Wako, C-200) with cyclohexane (Dojin, Luminazol) as developing solvent. The super special grade ethanol (Wako) and spectroscopic grade ethanol (Kishida Kagaku), and the deionized-doubly distilled water were used as solvents.

Apparatus

ESR spectra were recorded on an X-band spectrometer (Echo Electronics) combined with a JEOL JM-360

Table 2 Fluorescence quenching rate constants k_q of MV^{++} and BV^{++} and related parameters D' at 25°C[a]

Solvent EtOH vol%	[β-CyDx] / 10^{-2} M	MV^{++} k_q / 10^9 M^{-1} s^{-1}	MV^{++} D' / $(mPa\ s\ nm)^{-1}$	BV^{++} k_q / 10^9 M^{-1} s^{-1}	BV^{++} D' / $(mPa\ s\ nm)^{-1}$
10	0	8.0	4.5	7.1	3.8
10	1.0	3.1	3.4	1.5	2.6
50	0	4.1	2.3	3.8	1.9
50	1.0	3.9	1.7	2.2	1.3

[a] *D′ is defined by eq 3.*

electromagnetic with 100 kHz field modulation. Electronic absorption spectra were recorded on a UV-visible spectrophotometer (Shimadzu, MPS-50L). ICD spectra were recorded on a CD spectrophotometer (JASCO, J-500C) equipped with a data processor (JASCO, DP-501N). Fluorescence spectra were recorded on a Hitachi 650-40 spectrofluorometer. Fluorescence decays were measured by the photon counting technique, using a homemade nitrogen laser (337 nm) and a high speed transient recorder (Biomation 6500).

Procedures

The sample solutions were degassed by the freeze-pump-thaw method. For the radical preparation, the parent-compound concentrations were 1.0×10^{-3} M (M = mol dm^{-3}), while the CyDx concentrations were 1.0×10^{-2} M. $PBSQ^{-\cdot}$ was prepared by reduction with NaOH when the pH values of the sample solutions were kept at 8–9. $NB^{-\cdot}$ and NB-$d_5^{-\cdot}$ were prepared by reduction with $Na_2S_2O_4$ in the presence of a small amount of NaOH. $MV^{+\cdot}$ was prepared in 50% aqueous ethanol by UV light irradiation, since the radical was found to be most stable for a water fraction of 50%. $DHDPY^{+\cdot}$ was also prepared by UV light irradiation in 50% aqueous ethanol; NaCl (10 mg) was added to the sample solution (10 ml), and then a trace of dilute hydrochloric acid was added dropwise, keeping the solution within the pH range 3–4. In the fluorescence quenching measurements, the Py concentration was 5.0×10^{-7} and 5.0×10^{-6} M for 10% and 50% aqueous ethanol, respectively, while the maximum quencher concentrations were 1.0×10^{-3} M.

ACKNOWLEDGMENT

The authors are indebted to Professor Yukito Murakami, Professor Emeritus Seizo Misumi and Professor Tadashi Yonemitsu for the use of a circular dichroism spectrophotometer, and to Professors Kinshi Motomura and Yoshikiyo Moroi for the use of a spectrofluorometer.

REFERENCES

1 Kubozono, Y.; Ata, M.; Gondo, Y.; *Chem. Phys. Lett.* **1987**, *137*, 467.
2 Krishnamurthy, M.V.; Venkataraman, B.; *Indian J. Pure Appl. Phys.* **1967**, *5*, 325.
3 Okazaki, M.; Kuwata, K.; *J. Phys. Chem.* **1984**, *88*, 4181.
4 Ata, M.; Ph.D. Thesis, Kyushi Univ., Fukuoka, Japan, 1987.
5 Kuzunetsov, A.N.; Wasserman, A.M.; Volkov, A.U.; Korst, N.N.; *Chem. Phys. Lett.* **1971**, *12*, 103.
6 Flockhart, B.D.; Leith, I.R.; Pink, R.C.; *J. Chem. Soc., Chem. Commun.* **1966**, 885.
7 Kubozono, Y.; Aoyagi, M.; Ata, M.; Gondo, Y.; *Bull. Chem. Soc. Jpn.* **1990**, *63*, 3156.
8 Ata, M.; Suzuki, Y.; Kubozono, Y.; Aoyagi, M.; Gondo, Y.; *Chem. Phys. Lett.* **1989**, *157*, 19.
9 Ata, M.; Aoyagi, M.; Kubozono, Y.; Gondo, Y.; *Chem. Lett.* **1989**, 341.
10 Aoyagi, M.; Kubozono, Y.; Ata, M.; Gondo, Y.; *Chem. Phys. Lett.* **1986**, *131*, 201.
11 Harata, K.; Uedaira, H.; *Bull. Chem. Soc. Jpn.* **1975**, *48*, 375.
12 Shimizu, H.; Kaito, A.; Hatano, H.; *Bull. Chem. Soc. Jpn.* **1979**, *52*, 2678.
13 Shida, T.; Iwata, S.; *J. Phys. Chem.* **1971**, *75*, 2591.
14 Ishitani, A.; Kuwata, K.; Tsubomura, H.; Nagakura, S.; *Bull. Chem. Soc. Jpn.* **1963**, *36*, 1357.
15 Aoyagi, M.; Ph.D. Thesis, Kyushu Univ., Fukuoka, Japan, 1992.
16 Edward, J.T.; *J. Chem. Educ.* **1970**, *47*, 261. We adopted the formula, $b = (xyz)^{1/3}$ where x, y, and z are measurements of three axes of the molecular model at right angles to each other.
17 Birks, J.B.; Photophysics of Aromatic Molecules; John Wiley & Sons: New York, 1970.
18 Hashimoto, S.; Thomas, J.K.; *J. Am. Chem. Soc.* **1985**, *107*, 4655.